



UNIVERSITÀ  
DEGLI STUDI  
FIRENZE

# FLORE

## Repository istituzionale dell'Università degli Studi di Firenze

### **Magnetic Anisotropy of Tetrahedral Coll Single-Ion Magnets: Solid-State Effects**

Questa è la Versione finale referata (Post print/Accepted manuscript) della seguente pubblicazione:

*Original Citation:*

Magnetic Anisotropy of Tetrahedral Coll Single-Ion Magnets: Solid-State Effects / Sottini, Silvia; Poneti, Giordano; Ciattini, Samuele; Levesanos, Nikolaos; Ferentinos, Eleftherios; Krzystek, J.; Sorace, Lorenzo; Kyritsis, Panayotis. - In: INORGANIC CHEMISTRY. - ISSN 0020-1669. - STAMPA. - 55:(2016), pp. 9537-9548. [10.1021/acs.inorgchem.6b00508]

*Availability:*

The webpage <https://hdl.handle.net/2158/1056615> of the repository was last updated on 2021-03-22T15:23:01Z

*Published version:*

DOI: 10.1021/acs.inorgchem.6b00508

*Terms of use:*

Open Access

La pubblicazione è resa disponibile sotto le norme e i termini della licenza di deposito, secondo quanto stabilito dalla Policy per l'accesso aperto dell'Università degli Studi di Firenze (<https://www.sba.unifi.it/upload/policy-oa-2016-1.pdf>)

*Publisher copyright claim:*

La data sopra indicata si riferisce all'ultimo aggiornamento della scheda del Repository FloRe - The above-mentioned date refers to the last update of the record in the Institutional Repository FloRe

(Article begins on next page)

# Magnetic Anisotropy of Tetrahedral Co<sup>II</sup> Single Ion

## Magnets: Solid State Effects

Silvia Sottini,<sup>†</sup> Giordano Poneti,<sup>†,‡\*</sup> Samuele Ciattini,<sup>‡</sup> Nikolaos Levesanos,<sup>‡</sup> Eleftherios Ferentinos,<sup>‡</sup> J. Krzystek,<sup>||</sup> Lorenzo Sorace,<sup>†</sup> Panayotis Kyritsis<sup>‡\*</sup>

<sup>†</sup>University of Florence, Department of Chemistry "*Ugo Schiff*" and INSTM Research Unit of Florence, via della Lastruccia 3-13, 50019 Sesto Fiorentino, Italy.

<sup>‡</sup>Current address: Instituto de Química, Universidade Federal do Rio de Janeiro, Avenida Athos da Silveira Ramos 149, 21941-909 Rio de Janeiro, Brazil

<sup>‡</sup>University of Florence, Centro Interdipartimentale di Cristallografia Strutturale CRIST, via della Lastruccia 5, 50019 Sesto Fiorentino, Italy.

<sup>‡</sup>Inorganic Chemistry Laboratory, Department of Chemistry, National and Kapodistrian University of Athens, Panepistimiopolis, GR-15771 Athens, Greece.

<sup>||</sup>National High Magnetic Field Laboratory, Florida State University, Tallahassee, Florida 32310, United States.

**ABSTRACT.** This study reports the static and dynamic magnetic characterization of two mononuclear tetrahedral  $\text{Co}^{\text{II}}$  complexes,  $[\text{Co}\{^i\text{Pr}_2\text{P}(\text{E})\text{NP}(\text{E})^i\text{Pr}_2\}_2]$ ,  $\text{E} = \text{S}$  (**CoS<sub>4</sub>**),  $\text{Se}$  (**CoSe<sub>4</sub>**), which behave as single ion magnets. Low temperature (15 K) single crystal X-ray diffraction studies point out that the two complexes exhibit similar structural features in their first coordination sphere, but a disordered peripheral  $^i\text{Pr}$  group is observed only in **CoS<sub>4</sub>**. Although the latter complex crystallizes in an axial space group, the observed structural disorder leads to a larger transverse magnetic anisotropy for the majority of the molecules compared to **CoSe<sub>4</sub>**, as it is confirmed by EPR spectroscopy. Static magnetic characterization indicates that both **CoS<sub>4</sub>** and **CoSe<sub>4</sub>** show easy axis anisotropy, with comparable  $D$  values ( $\sim -30 \text{ cm}^{-1}$ ). Moreover, alternating current (ac) susceptibility measurements on these  $\text{Co}^{\text{II}}$  complexes, magnetically diluted in their isostructural  $\text{Zn}^{\text{II}}$  analogues, highlight the role of dipolar magnetic coupling in the mechanism of magnetization reversal. In addition, our findings suggest that, despite their similar anisotropic features, **CoS<sub>4</sub>** and **CoSe<sub>4</sub>** relax magnetically via different processes. This work provides experimental evidence that solid state effects may affect the magnetic behavior of single ion magnets.

## INTRODUCTION

The discovery in the 1990s that some multinuclear transition metal clusters, referred to as single molecule magnets (SMMs), exhibit slow relaxation of magnetization has been a hallmark in the field of molecular magnetism.<sup>1-2</sup> Thanks to their magnetic ground state with a preferential magnetization direction (easy axis anisotropy), these materials display an activation barrier to the relaxation of their magnetization of pure molecular origin. This allows them to retain magnetic information at low temperature and to show quantum effects like quantum tunneling of the magnetization (QTM)<sup>3</sup> and parity effects.<sup>4</sup> For these reasons SMMs are widely investigated as potential materials either for ultra high-density information-storage,<sup>5</sup> molecular spintronics<sup>6</sup> or quantum computation devices.<sup>7</sup> More recently, a closely related behavior was found in mononuclear complexes of lanthanides,<sup>8</sup> actinides<sup>9</sup> and transition metals.<sup>10-12</sup> The reduced complexity of the latter systems, known as single ion magnets (SIMs), combined with a large range of zero-field splitting (ZFS) values,<sup>10-14</sup> suggested a potentially easier chemical tuning of their magnetic anisotropy<sup>15-17</sup> compared to multinuclear systems.<sup>18-21</sup> As a result, during the last few years, significant research efforts have been devoted to master a synthetic control over the magnetic anisotropy of SIMs containing 3d-metal ions.<sup>10-12</sup>

The first mononuclear 3d-metal-based SIM ever reported has been a trigonal pyramidal high-spin Fe<sup>II</sup> complex.<sup>22</sup> Following that report, slow magnetic relaxation has been established for a large number of complexes containing 3d-metal ions such as Cr<sup>II</sup>,<sup>23-24</sup> Mn<sup>III</sup>,<sup>25-33</sup> Fe<sup>I</sup>,<sup>34-36</sup> Fe<sup>II</sup>,<sup>37-42</sup> Fe<sup>III</sup>,<sup>29,43</sup> Co<sup>I</sup>,<sup>44</sup> Ni<sup>II</sup><sup>45-46</sup> and Ni<sup>I</sup>.<sup>47-48</sup> In addition to these, a large number of Co<sup>II</sup>-based SIMs has been recently identified, following the report on the archetypal tetrahedral (PPh<sub>4</sub>)<sub>2</sub>[Co(SPh)<sub>4</sub>] system, the first mononuclear Co<sup>II</sup> complex showing slow relaxation of the magnetization in the absence of an external magnetic field.<sup>49</sup> Indeed, Co<sup>II</sup> complexes constitute to date the largest

family of 3d-metal-based mononuclear SIMs, exhibiting a large variety of first coordination sphere and of magnetic anisotropy types,<sup>29,39,50-79</sup> as recently reviewed<sup>10,12,14</sup> (and references therein).

Up to now, however, experimental<sup>50,51</sup> and computational investigations<sup>16</sup> of the magnetic anisotropy in Co<sup>II</sup>-based SIMs has been carried out by mainly taking into account the electronic and structural features of solely the first coordination sphere of the investigated complexes. For example, for the (PPh<sub>4</sub>)<sub>2</sub>[Co(EPh)<sub>4</sub>], E = O, S, Se, series of complexes, Co<sup>II</sup>–E covalency effects have been discussed, suggesting the importance of soft donor ligands in the pursuit of systems with a large magnetic anisotropy.<sup>53</sup> This series of complexes has recently been computationally investigated, in an effort to probe effects based on the nature of the E donor atoms.<sup>80</sup>

In this work we demonstrate, through a multi-technique approach involving variable temperature X-ray diffraction analysis and High-Frequency and -Field EPR (HF-EPR) spectroscopy, that subtle structural effects in peripheral groups far away from the metal center may play a significant role in determining the rhombic distortion of the anisotropy tensor in SIMs, a crucial parameter in the relaxation of the magnetization.<sup>1</sup> Towards this aim, we report here the investigation of two CoL<sub>2</sub> complexes bearing the deprotonated L<sup>−</sup> form of LH chalcogenated imidodiphosphate, R<sub>2</sub>P(E)NHP(E)R<sub>2</sub>, type of ligands (R = various alkyl or aryl groups; E = O, S, Se, Te), which are regarded as inorganic analogues of β-diketonates.<sup>81-84</sup> More specifically, we investigated [Co{<sup>i</sup>Pr<sub>2</sub>P(E)NP(E)<sup>i</sup>Pr<sub>2</sub>}<sub>2</sub>], E = S, Se (hereafter denoted as **CoS<sub>4</sub>** and **CoSe<sub>4</sub>**, respectively), which have been previously reported by Gilby and Piggott to coordinate Co<sup>II</sup> in a distorted tetrahedral geometry.<sup>85</sup> Tetrahedral complexes of this type containing Co<sup>II</sup>S<sub>4</sub> coordination spheres and Ph, <sup>i</sup>Pr or Ph/<sup>i</sup>Pr as R groups have already been investigated by some of

us.<sup>86</sup> In particular, variable frequency EPR and W-band ENDOR investigations provided accurate spin Hamiltonian (SH) parameters for these  $S = 3/2$  systems,<sup>87-88</sup> subsequently interpreted via *ab initio* quantum chemical methods.<sup>89</sup> Based on the latter work, the **CoS<sub>4</sub>** and **CoSe<sub>4</sub>** complexes are predicted to exhibit large easy axis anisotropy. The chemical versatility imposed by the nature of the donor E atoms (S or Se), combined with the observed different orientations of the peripheral <sup>i</sup>Pr groups in **CoS<sub>4</sub>** and **CoSe<sub>4</sub>** (*vide infra*), allowed us to probe effects of the first and second coordination sphere on their magnetic anisotropy. This is the second report on 3d-metal-based SIMs bearing [R<sub>2</sub>P(E)NP(E)R<sub>2</sub>]<sup>−</sup> type of ligands, following that of the octahedral  $S = 2$  [Mn{Ph<sub>2</sub>P(O)NP(O)Ph<sub>2</sub>}<sub>3</sub>] complex.<sup>27</sup>

## MATERIALS AND METHODS

### Synthesis

The <sup>i</sup>Pr<sub>2</sub>P(E)NHP(E)<sup>i</sup>Pr<sub>2</sub>, E = S, Se,<sup>90</sup> ligands and the corresponding [M{<sup>i</sup>Pr<sub>2</sub>P(E)NP(E)<sup>i</sup>Pr<sub>2</sub>}<sub>2</sub>] complexes, M = Co, E = S, Se;<sup>85</sup> M = Zn, E = S,<sup>91-92</sup> Se,<sup>91</sup> were prepared according to published procedures. The magnetically diluted systems (hereafter denoted as **Co/ZnS<sub>4</sub>** and **Co/ZnSe<sub>4</sub>**) were prepared by dissolving in CH<sub>2</sub>Cl<sub>2</sub> the appropriate amounts, respectively, of **CoS<sub>4</sub>** and **CoSe<sub>4</sub>** with their Zn<sup>II</sup> counterparts, followed by coprecipitation via the addition of 15-fold amount of *n*-hexane and subsequent rigorous stirring.

### Electronic Spectroscopy

UV-vis reflectance spectra were acquired at room temperature using a Jasco V-670 spectrophotometer equipped with an integrating sphere.

## X-ray crystallography

The single crystals were mounted in air on a glass fiber. The intensities' data for **CoS<sub>4</sub>** and **CoSe<sub>4</sub>** were collected at 110 K and 15 K using a Helijet head (Oxford Diffraction) on an Oxford Diffraction Excalibur diffractometer equipped with Mo K $\alpha$  radiation. In all cases, the programs CrysAlis CCD and CrysAlis RED were used for the data collection and the data reduction. The structures were solved using the SIR-97 package<sup>93</sup> and subsequently refined on the F<sup>2</sup> values by the full-matrix least-squares program SHELXL-97.<sup>94</sup> In all cases, the non-hydrogen atoms, except those of the *i*Pr moiety, where disorder occurs, were anisotropically refined. The hydrogen atoms were found in the Fourier difference map. X-ray powder diffraction measurements were carried out at room temperature in air by using a Bruker New D8 Da Vinci diffractometer (Cu-K $\alpha$  radiation, 40 kV  $\times$  40 mA), equipped with a Bruker LYNXEYE-XE detector, scanning range  $2\theta = 3\text{--}50^\circ$ ,  $0.02^\circ$  increments of  $2\theta$ , and a counting time of 0.8 s/step.

## Electron Paramagnetic Resonance

HFEPR measurements were performed at the National High Magnetic Field Laboratory at several sub-THz frequencies between 52 and 406 GHz and low temperatures on loose powders and pellets, using an instrument described in detail in Hassan *et al.*,<sup>95</sup> with the exception of a Virginia Diodes sub-THz wave source, consisting of a  $13\pm 1$  GHz frequency generator and a cascade of amplifiers and frequency multipliers.

## Magnetometry

Samples used for direct current (dc) and alternating current (ac) magnetic investigations consisted of pellets made out of microcrystalline powders of complexes **CoS<sub>4</sub>** and **CoSe<sub>4</sub>**, as well as the corresponding solid solutions **Co/ZnS<sub>4</sub>** and **Co/ZnSe<sub>4</sub>**. Direct current magnetic

investigations were performed using a Quantum Design MPMS instrument equipped with a 5 T magnet. The temperature dependence of the magnetization ( $M$ ) was followed from 1.8 to 300 K by applying a 1 T field ( $B$ ) from 300 to 45 K and a 0.1 T field below 45 K to reduce magnetic saturation effects. Magnetic susceptibility per mole ( $\chi_M$ ) was then evaluated as  $\chi_M = M/B$ . Alternating current magnetic susceptibility analysis was performed with a Quantum Design PPMS setup working in the 10 – 10000 Hz range or with a Quantum Design MPMS instrument working in the 10 – 1000 Hz range with zero, 1 kOe or 2 kOe applied static field. Magnetic data were corrected for the sample holder contribution and for the sample diamagnetism using Pascal's constants. The ac susceptibility data were analyzed within the extended Debye model,<sup>96-97</sup> in which a maximum in the out-of-phase component  $\chi_M''$  of the complex susceptibility is observed when the relaxation time  $\tau$  equals  $(2\pi\nu)^{-1}$ . The frequency dependence of  $\chi_M''$  at constant temperature was here fitted using equation (1):

$$\chi_M''(\omega) = (\chi_T - \chi_S)[(\omega\tau)^{1-\alpha}\cos(\alpha\pi/2)]/[1 + 2(\omega\tau)^{1-\alpha}\sin(\alpha\pi/2) + (\omega\tau)^{2-2\alpha}] \quad (1)$$

where  $\omega = 2\pi\nu$ ,  $\chi_T$  and  $\chi_S$  are the isothermal and adiabatic susceptibilities, *i.e.*, the susceptibilities observed in the two limiting cases  $\nu \rightarrow 0$  and  $\nu \rightarrow \infty$ , respectively, and  $\alpha$  is a parameter which accounts for a distribution of relaxation times.

## RESULTS & DISCUSSION

### X-ray crystallography

Complexes **CoS<sub>4</sub>** and **CoSe<sub>4</sub>** had been earlier structurally characterized by crystallographic studies at room temperature.<sup>85</sup> In the work presented herein, the crystal structures of these

complexes were solved and refined at 15 K and 110 K to investigate differences in structural features that might be relevant in determining the low temperature dynamics of magnetization. The crystal data and the structural refinement parameters, as well as the CCDC deposition numbers, are listed in Table S1 [Supporting Information (SI)]. Selected bond lengths and angles at the two temperatures for the two complexes are listed in Table 1, along with the corresponding parameters reported in literature for room temperature (RT) structures.<sup>85</sup>

**Table 1.** Selected bond lengths, angles and closest Co  $\cdots$  Co intermolecular distances for **CoS<sub>4</sub>** and **CoSe<sub>4</sub>**, at 15 K, 110 K and RT.

	<b>CoS<sub>4</sub></b> 15 K	<b>CoS<sub>4</sub></b> 110 K	<b>CoS<sub>4</sub></b> RT <sup>85</sup>	<b>CoSe<sub>4</sub></b> 15 K	<b>CoSe<sub>4</sub></b> 110 K	<b>CoSe<sub>4</sub></b> RT <sup>85</sup>
av. Co–E (Å)	2.3129	2.3182	2.3172	2.4319	2.4358	2.4350
av. E–P (Å)	2.0287	2.0349	2.0278	2.1823	2.1863	2.1788
av. P–N (Å)	1.5870	1.5898	1.5831	1.5930	1.5948	1.5953
Closest Co $\cdots$ Co (Å)	8.520	8.549	8.669	8.918	8.942	8.990
av. P–N–P (°)	137.4	138.2	138.3	137.6	137.7	137.9
av. $\xi$ (°)	90	90	90	89.24	88.81	88.62
av. E–Co–E (°)	110.83	110.93	110.48	112.03	111.94	112.02
	108.79	108.75	108.97	108.20	108.24	108.21
av. P–E–N (°)	139.6	141.4	140.2	131.7	131.9	132.1
av. $\omega$ (°)	164.6	165.2	164.8	162.9	163	163.1

The space group in which the molecules crystallize is different in the two cases, and is the same observed at room temperature:<sup>85</sup>  $I4_1/a$  for **CoS<sub>4</sub>** and  $P-1$  for **CoSe<sub>4</sub>**. More relevant, for our scope, is the fact that in **CoS<sub>4</sub>** the Co atom sits on a  $S_4$  symmetry axis, whereas **CoSe<sub>4</sub>** has no symmetry at all. Notwithstanding these differences, the structure of the first coordination sphere of both complexes at 110 K is very similar, their core being arranged in a distorted tetrahedral geometry as shown in Figure 1. The dihedral angle between the two E-Co-E endocyclic planes (denoted herein as  $\xi$ ) is a measure of the deviations from an ideal tetrahedral first coordination sphere. In that respect, **CoS<sub>4</sub>** exhibits the  $\xi$  value ( $90^\circ$ ) of the ideal tetrahedral symmetry at all temperatures investigated, due to the  $I4_1/a$  symmetry group, whereas **CoSe<sub>4</sub>** shows slightly smaller values. However, these deviations are remarkably diminished as the temperature is lowered (Table 1).

It should be noted that the magnitude of the E-Co-E-P torsion angle  $\omega$  of **CoS<sub>4</sub>** and **CoSe<sub>4</sub>** (Table 1) is very close to that ( $180^\circ$ ) of the ideal  $D_{2d}$  symmetry. Therefore, the chelating  $L = [R_2P(E)NP(E)R_2]^-$  ligands of the two complexes seem to intrinsically lead to  $CoL_2$  complexes exhibiting close to  $D_{2d}$  structures when their peripheral groups R are the same, i.e. only Ph<sup>89</sup> or only <sup>*i*</sup>Pr (this work). In addition to packing effects of these bulky ligands, the distortion from the ideal tetrahedral geometry of  $Co^{II}E_4$ -containing complexes,  $E = S, Se$ , is also affected by intra- and inter- molecular interactions between the soft E donor atoms, as discussed for  $[Co(SPh)_4]^{2-}$ .<sup>98</sup> Therefore, the observed geometries of **CoS<sub>4</sub>** and **CoSe<sub>4</sub>**, which cannot be accounted for by Jahn-Teller distortions, seem to be conferred by the  $Co^{II}$ -coordinated  $L^-$  chelating ligands and their soft donor atoms.

As expected, the Co–Se bonds lengths are slightly larger than the corresponding Co–S ones. Moreover, the Co–S bonds of **CoS<sub>4</sub>** are all crystallographically equivalent to each other, whereas

only minor deviations (0.01-0.2 %) from the average Co–Se bond length occur for **CoSe<sub>4</sub>**. At 15 K, for both complexes, the relevant bond lengths reported in Table 1 slightly decrease. Finally, we note that the average E-Co-E-P torsion angle ( $\omega$ ) for the E atoms belonging to the same ligand diminishes as the temperature is lowered, more evidently for **CoS<sub>4</sub>**. This is quite relevant since a previously performed computational investigation of similar Co<sup>II</sup> systems, has revealed the dependence of their magnetic anisotropy on  $\omega$ .<sup>89</sup>

Looking beyond the first coordination sphere, we note that some more relevant differences occur in the arrangement of the <sup>i</sup>Pr peripheral groups. In particular for **CoS<sub>4</sub>**, at both 15 K and (even if less evidently) at 110 K, structural disorder is observed at the position of a C atom in one of the <sup>i</sup>Pr groups of the asymmetric unit, refined with occupancy factors of 0.744/0.256 at 15 K and 0.857/0.143 at 100 K. This phenomenon, which was not revealed in the previously reported room temperature structure,<sup>85</sup> implies that while the crystal fulfills the requirements for tetragonal symmetry, the disorder results in molecules exhibiting different conformations. The relative abundance of these conformations can be calculated assuming statistical distribution based on occupancy factors, so that only a fraction (31 %) of the molecules are strictly tetragonal (Table 2). This symmetry lowering may have important consequences in determining the magnetic behavior at low temperature (*vide infra*).<sup>99-101</sup>

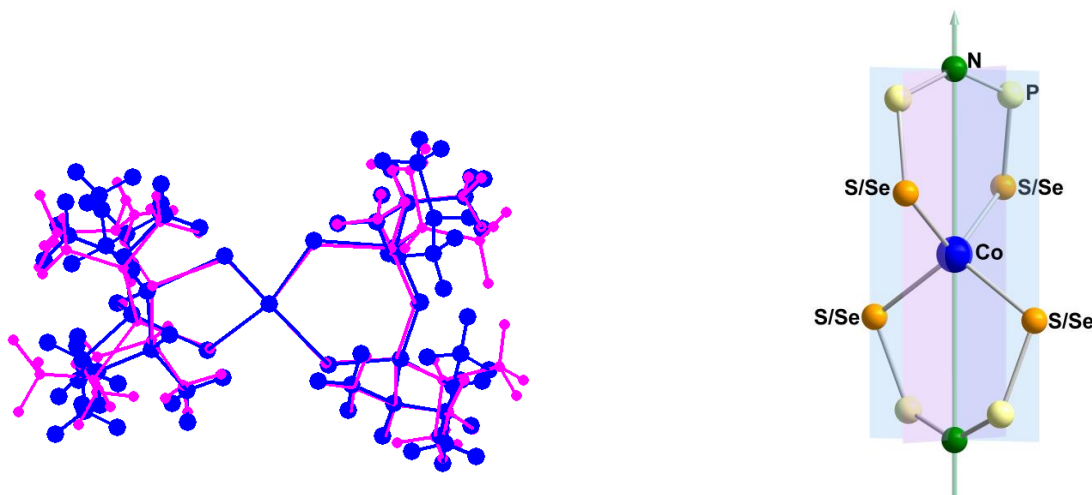


**Figure 1.** Left: Overlaid molecular structures of **CoS<sub>4</sub>** (magenta) and **CoSe<sub>4</sub>** (blue) at 110 K, showing the differences in the second coordination sphere of the complexes. Right: detail of the **Co<sup>II</sup>** coordination sphere. The  $\omega$  dihedral angle is the one formed by the S/Se-Co-S/Se and Co-S/Se-P planes, whereas the  $\xi$  one is formed by the two S/Se-Co-S/Se endocyclic planes.

**Table 2.** Statistical abundance of the different conformers calculated on the basis of the Site Occupation Factor (SOF) obtained by X-ray structure resolution at 15 K for **CoS<sub>4</sub>**. A is referring to the major occupancy (0.744) and B to the minor one (0.256).

Conformer type	Statistical abundance	Tetragonal system
AAAA	30.6 %	YES
AAAB	42.2 %	NO
AABB	21.8 %	NO
ABBB	5 %	NO
BBBB	0.4 %	YES

## EPR spectroscopy

EPR spectra of a loose polycrystalline sample of **CoS<sub>4</sub>** consist of a single resonance of a derivative shape, observed at low temperatures (4.5 – 10 K) throughout the whole investigated frequency range (9.5 and 52 – 406 GHz). The shape of this signal is what one expects from a single crystal and strongly suggests a phenomenon known as field-induced alignment or torquing, observed in the polycrystalline sample subjected to a high magnetic field, typically along the axis corresponding to the maximum anisotropy of the ZFS tensor (i.e. easy axis *z*). This phenomenon was early on observed in HFEPR spectra of polycrystalline SMMs<sup>102-105</sup> and can be used to the experimenter's advantage if no single crystals of sufficient size or quality are available. Figure 2a shows such a quasi-single crystal spectrum at 203.2 GHz and 4.5 K, with its simulation. A complete multifrequency set of HFEPR spectra taken at the same temperature is shown in Figure S1 (SI).

Magnetic properties of an  $S = 3/2$  spin system like **CoS<sub>4</sub>** can in principle be described by a SH that includes the ZFS term and the electron Zeeman interaction:

$$H_s = D\vec{S}_z^2 + E(\vec{S}_x^2 - \vec{S}_y^2) + \mu_B \vec{B} * g * \vec{S} \quad (2)$$

where  $\vec{S}$  represents the electron-spin angular momentum operator,  $D$  and  $E$  are the axial and rhombic ZFS parameters, respectively, and  $g$  is the Zeeman anisotropic interaction tensor with principal values  $g_x$ ,  $g_y$  and  $g_z$ . In the following, we will refer to the two Kramers doublets as  $M_S = \pm 1/2$  and  $M_S = \pm 3/2$ .

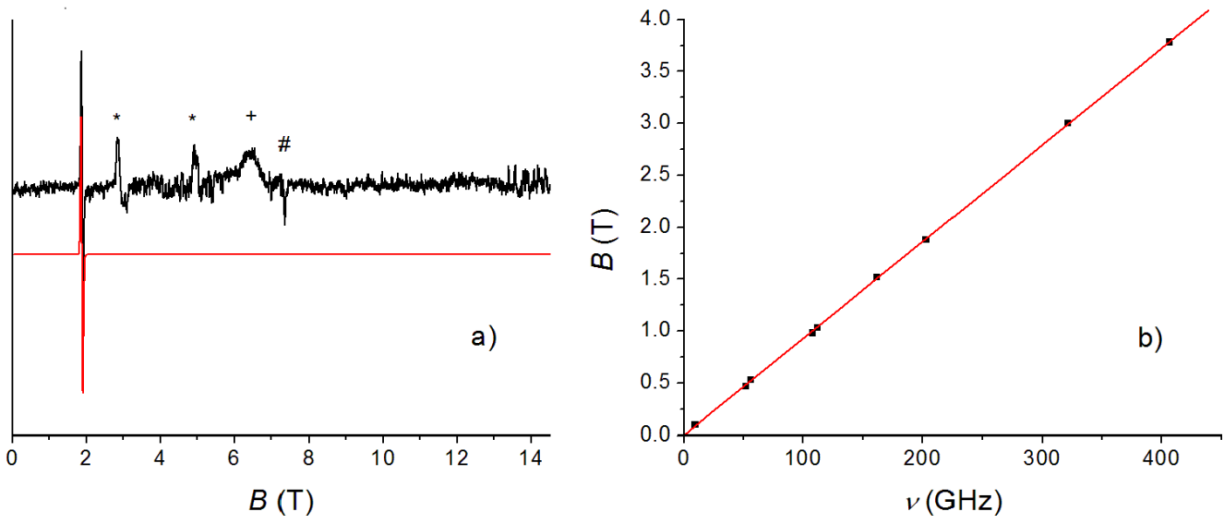


**Figure 2.** (a) HFEPR spectrum of **CoS<sub>4</sub>** powder at 203.2 GHz and 4.5 K (black trace) and its simulation (red trace) assuming a single crystal-like orientation along the easy axis of the ZFS tensor forced by field torquing, and using the  $S = 3/2$  SH parameters as in Table 3 with the exception of  $g = 2.56$ . The asterisks identify the signals due to solid molecular dioxygen, the plus sign marks the signal of the probe and the hash sign denotes a  $g = 2$  impurity; neither of those is simulated. (b) Frequency dependence of the EPR resonance in **CoS<sub>4</sub>** at 4.5 K (black squares), and the corresponding linear fit (red line) using an effective  $S^{eff} = 1/2$  SH with  $g_z^{eff} = 7.68$ .

An analysis of the frequency dependence of the resonance field of the only observed line in **CoS<sub>4</sub>** (Figure 2b) clearly evidences that it corresponds to an intra-Kramers transition within one of the two Kramers doublets, since the intercept of the linear regression is zero (*i.e.*, no zero field interaction is affecting - in first order - the magnitude of resonance field). The observed EPR spectra can be then interpreted by considering only the lower energy doublet and thus assuming

an effective  $S^{eff} = 1/2$  with strongly anisotropic  $g$  values. It follows from the linear fit in Figure 2b that the EPR signal of **CoS<sub>4</sub>** is characterized by  $g_z^{eff} = 7.68$ , while the corresponding  $g_x^{eff}$  and  $g_y^{eff}$  transitions were not detected. The dependence of the effective  $g$  values of the  $S^{eff} = 1/2$  system on the intrinsic  $g$  values and the ZFS parameters of the  $S = 3/2$  system, are well known.<sup>87,106</sup>

$$\begin{aligned} g_x^{eff} &= g_x \left( 1 \pm \frac{1-3\lambda}{\sqrt{1+3\lambda^2}} \right) \\ g_y^{eff} &= g_y \left( 1 \pm \frac{1+3\lambda}{\sqrt{1+3\lambda^2}} \right) \\ g_z^{eff} &= g_z \left( 1 \mp \frac{2}{\sqrt{1+3\lambda^2}} \right) \end{aligned} \tag{3}$$

where  $\lambda = E/D$  and in each equation the upper sign is valid for easy plane anisotropy ( $D > 0$ ,  $M_S = \pm 1/2$  ground state), while the lower sign applies for easy axis anisotropy ( $D < 0$ ,  $M_S = \pm 3/2$  ground state). Only by choosing the lower sign (and thus easy axis type anisotropy) in the above equations, and assuming  $g_z > 2.5$  and negligible  $\lambda$ , it is possible to obtain  $g_z^{eff} = 7.68$ . The sign of  $D$  is thus clearly determined as negative. It is evident, however, that the observation of such an EPR signal requires the rhombicity factor  $\lambda$  to be different from zero. Indeed, the rhombic  $E$  component of the ZFS mixes the  $M_S = \pm 1/2$  and  $M_S = \pm 3/2$  states in the magnetic sublevels of the Kramers doublets. This mixing of states results in a non-zero transition probability of the otherwise forbidden  $\Delta M_S = \pm 3$  transition, and provides evidence for a breakdown of the tetragonal molecular symmetry, as found by the low temperature X-ray study (*vide supra*).

Measurements performed on a pelletized sample (Figure S2, SI), which resulted in a change of its shape and decrease of intensity, confirmed that the single-crystal-like shape of the observed

EPR line in **CoS<sub>4</sub>** is due to a field-induced alignment of the polycrystalline powder with  $B \parallel z$ . The corresponding perpendicular turning points ( $B \parallel x$  and  $y$ ) in a pellet, however, were not found. The simulated field/frequency dependence (Figure S3, SI) shows that for a large  $|D|$  and very small rhombicity of the ZFS tensor these points would appear at prohibitively high fields, even at the lowest frequencies available. Following these considerations, the spectra at different frequencies of the loose powders could be well reproduced by simulations assuming a single crystal-like orientation with magnetic field parallel to the easy axis (see Figure 2a). The best simulations were obtained using  $g_z = 2.56$ , which is reasonable for tetrahedral  $\text{Co}^{\text{II}}$  systems, an arbitrarily large magnitude of the  $D$  parameter ( $|D| \geq 30 \text{ cm}^{-1}$ ), and an equally arbitrarily small rhombicity factor  $|E/D| = 0.01$ , which is about the lower limit necessary for the nominally forbidden  $\Delta M_S = \pm 3$  transition to be detectable. Regarding the absolute value of  $|D|$ , the lack of inter-Kramers-doublet transitions in the high-frequency measurements implies it is greater than  $20 \text{ cm}^{-1}$ . Along the same lines, the non-observation of the intra-doublet  $\Delta M_S = \pm 1$  transition at higher temperatures is not surprising, since at the temperatures needed to appreciably populate the higher energy  $M_S = \pm 1/2$  Kramers doublet, relaxation effects apparently weaken and/or broaden this resonance beyond detectability.

Unlike its sulfur analog, **CoSe<sub>4</sub>** was EPR-silent at all the microwave frequencies and temperatures investigated. This points out that similar indications concerning the magnitude of  $D$  as in **CoS<sub>4</sub>** are expected to hold also for **CoSe<sub>4</sub>**, but in this case the ZFS tensor is even more axial, *i.e.* the  $|E/D|$  ratio is lower than that of **CoS<sub>4</sub>**, leading to an immeasurably small transition probability of the  $\Delta M_S = \pm 3$  intra-doublet transition. The observed EPR behavior indicates that, despite occurring in the second coordination sphere, the deviation from strict tetragonal symmetry in **CoS<sub>4</sub>** is enough to induce a non-zero transition probability for the ground Kramers'

intra-doublet,  $\Delta M_S = \pm 3$ , transition, due to the existence of a non-zero rhombic component  $E$  of the ZFS tensor.

### Direct current magnetic characterization

The temperature dependence of the  $\chi_M T$  product of polycrystalline samples of **CoS<sub>4</sub>** and **CoSe<sub>4</sub>**, measured in the 2-300 K range, is shown in Figure 3. The room temperature  $\chi_M T$  values of both compounds (2.55 emuK/mol for **CoS<sub>4</sub>** and 2.72 emuK/mol for **CoSe<sub>4</sub>**) are larger than the one predicted for Curie  $S = 3/2$  spins with  $g = 2.00$  (1.875 emuK/mol), indicating the presence of a significant spin-orbit coupling with low-lying excited states, as expected.<sup>106</sup> Upon cooling at temperatures below 100 K, both compounds display a decrease in their  $\chi_M T$  values, the origin of which may be found in the ZFS of their  $S = 3/2$  ground state or in antiferromagnetic intermolecular interactions. The contribution of the latter are considered to be negligible due to the large Co  $\cdots$  Co intermolecular distances observed in the crystal lattice of the two complexes (Table 1). The field dependence of the magnetization of **CoS<sub>4</sub>** and **CoSe<sub>4</sub>**, reported in the inset of Figure 3 (see Figure S4, SI, for 2.5 and 4.5 K data), displays no saturation at 1.9 K, reaching 2.12 and 2.16  $\mu_B$ /mol at 5 T, respectively.

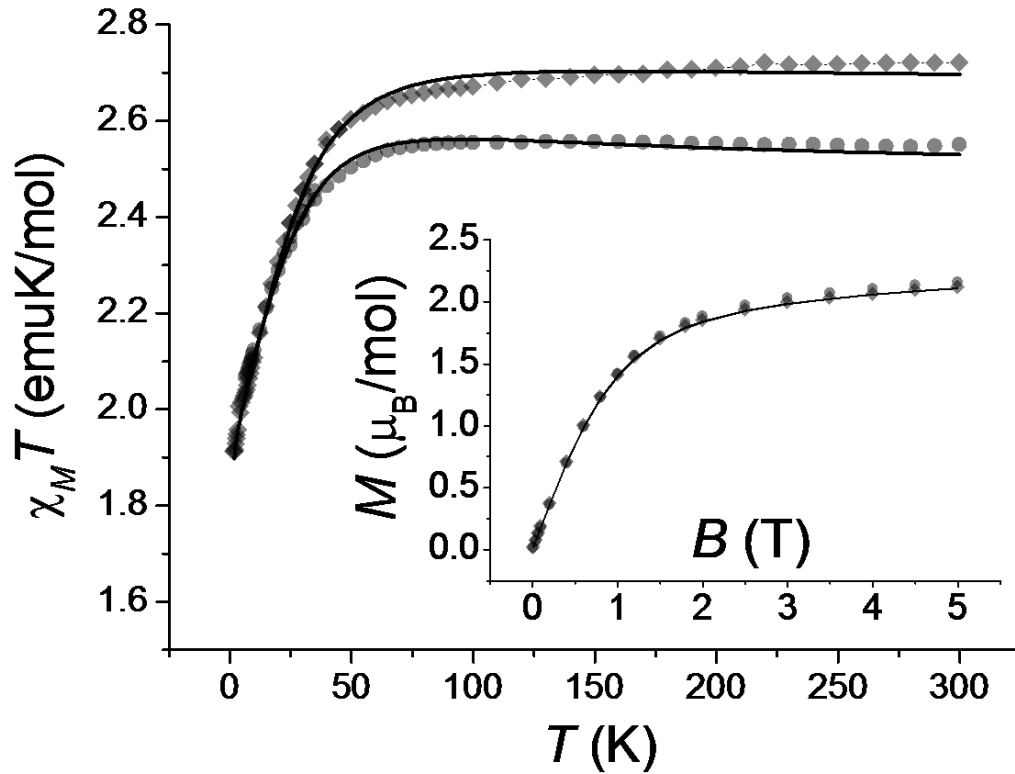


**Figure 3.** Temperature dependence of the  $\chi_M T$  product for the **CoS<sub>4</sub>** (full grey circles) and **CoSe<sub>4</sub>** (full grey lozenges). *Inset:* Magnetization *versus* magnetic field of **CoS<sub>4</sub>** (full grey circles) and **CoSe<sub>4</sub>** (full grey lozenges) taken at 1.9 K. In both panels the lines are the results of the best fitting procedure with the SH (eq. 2) and parameters described in the text.

In order to obtain a quantitative estimation of the magnetic anisotropy parameters of **CoS<sub>4</sub>** and **CoSe<sub>4</sub>**,  $M(B)$  and  $\chi_M T(T)$  were fitted with the PHI program<sup>108</sup> according to the SH (eq. 2). The parameters obtained from the best-fitting procedure of the data are listed in Table 3; the corresponding curves are displayed as solid lines in Figures 3 and S4 (SI).

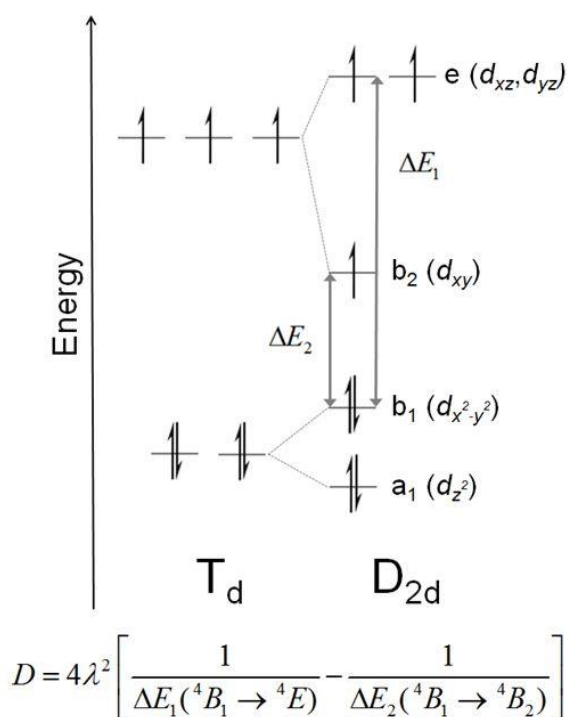
**Table 3.** SH parameters for **CoS<sub>4</sub>** and **CoSe<sub>4</sub>**, estimated by the fit to the dc magnetic measurements.

	$g$	$D$ (cm <sup>-1</sup> )	$E$ (cm <sup>-1</sup> )	$ E/D $
<b>CoS<sub>4</sub></b>	2.29	-30.5	0.07	0.0023
<b>CoSe<sub>4</sub></b>	2.38	-30.4	0.05	0.0016

The results obtained by static magnetization data of both **CoS<sub>4</sub>** and **CoSe<sub>4</sub>** are in line with the HFEPR analysis: the obtained  $g$  and the negative  $D$  values describe a substantial easy-axis character of the magnetic anisotropy for both systems at low temperature. As a confirmation, fitting procedures imposing positive  $D$  values yielded significantly poorer results. Furthermore, the observation of an easy axis type anisotropy is in line with computational expectations, which, for the  $\omega$  torsion angles listed in Table 1, predict very large negative  $D$  values and a small rhombicity.<sup>89</sup> The minor differences in the  $E$  parameter and  $|E/D|$  ratio of **CoS<sub>4</sub>** and **CoSe<sub>4</sub>**, even if in line with the HFEPR results, cannot be regarded as physically relevant, due to the lower sensitivity of magnetometry in the determination of transverse anisotropy terms compared to spectroscopic techniques, thus essentially describing the two systems as magnetically axial.

The obtained SH parameters fall within the range of previously characterized mononuclear tetrahedral Co<sup>II</sup> complexes containing chalcogenides as donor atoms, either fully<sup>53,80</sup> or in part.<sup>50</sup> However, unlike previous studies reporting a correlation between the absolute value of the  $D$  parameter and the softness of the chalcogenido donor atoms,<sup>50,53</sup> this does not seem to be the case in our systems, for which the estimated  $D$  value is essentially the same for **CoS<sub>4</sub>** and **CoSe<sub>4</sub>**. This could not be *a priori* proposed on the basis of an exclusive consideration of the electronic

effects of the Co–S/Se bonding on the magnetic anisotropy of Co<sup>II</sup>. Indeed, a ligand imposing a weaker ligand field on Co<sup>II</sup> would be expected to induce an increase of the absolute value of the  $D$  parameter in tetrahedral Co<sup>II</sup> complexes.<sup>53,80</sup> This effect can be qualitatively understood by looking at Scheme 1, where the combined effect of ligand field strength, distortion from the T<sub>d</sub> to D<sub>2d</sub> geometry and spin-orbit coupling on the anisotropy of tetrahedral Co<sup>II</sup> complexes is pictorially represented.



Scheme 1. Energy pattern (not in scale) of d-orbitals for Co<sup>II</sup> complexes in T<sub>d</sub> and D<sub>2d</sub> symmetry, showing the energy differences affecting the  $D$  value in perturbation theory, according to the reported equation. In this equation,  $\lambda$  is the spin-orbit coupling constant.

In this case, perturbation theory predicts that the  $D$  values are influenced by the lowest electronic excitation energies, as described in Scheme 1. While in  $T_d$  symmetry no second-order magnetic anisotropy is expected as a consequence of cubic symmetry, distortion of the first coordination sphere yielding a  $D_{2d}$  geometry affords distinct excitation energies from the  $d_{x^2-y^2}$  orbital (transforming as  $b_1$  in  $D_{2d}$  symmetry) to the  $d_{xy}$  ( $b_2$ ) and to  $d_{xz}$  or  $d_{yz}$  orbitals ( $e$ ). Consequently, the larger contribution of the spin-orbit coupling to the magnetic anisotropy arises mainly from the single electron excitation  $d_{x^2-y^2} \rightarrow d_{xy}$ , leading to a more negative  $D$  value, as the energy difference of these two orbitals ( $\Delta E_2$ , Scheme 1) is diminished.<sup>89,109</sup> Further lowering of the symmetry, removing the degeneracy of  $d_{xz}$  and  $d_{yz}$ , would provide a degree of rhombicity to the anisotropy.

In the present case, UV-vis reflectance spectra of **CoS<sub>4</sub>** and **CoSe<sub>4</sub>** reveal small differences in their d-d transitions (Figure S5, SI), which, by analogy to the spectra of  $[\text{Co}\{\text{R}_2\text{P}(\text{S})\text{NP}(\text{S})\text{R}_2\}_2]^{86,110}$  or  $[\text{Co}(\text{XPh})_4]^{2-}$ ,  $\text{X} = \text{O}, \text{S}, \text{Se}$ ,<sup>53,80,111</sup> indicate that the ligand field in **CoSe<sub>4</sub>** is indeed weaker than that of **CoS<sub>4</sub>**. However, no trend in the magnitude of the  $D$  parameter of the two complexes, as estimated by magnetometry, is evident. Extensive *ab initio* calculations have recently revealed that a large number of parameters affect the sign and magnitude of the ZFS in the  $[\text{Co}(\text{XPh})_4]^{2-}$  complexes.<sup>80</sup> Similar studies on **CoS<sub>4</sub>** and **CoSe<sub>4</sub>** would be needed to disentangle symmetry and metal-ligand bonding contributions to their magnetic anisotropy, but they are beyond the scope of the present work. A recent computational investigation of the  $[\text{Co}\{\text{R}_2\text{P}(\text{S})\text{NP}(\text{S})\text{R}_2\}_2]$  complexes,  $\text{R} = \text{Ph}$  or  $\text{Ph}^i\text{Pr}$ , has revealed a dependence of their magnetic anisotropy on the S-Co-S-P torsion angle  $\omega$ ,<sup>89</sup> in line with our experimental observations for **CoS<sub>4</sub>** and **CoSe<sub>4</sub>**.

## Alternating current magnetic characterization

The dynamics of the magnetization of **CoS<sub>4</sub>** and **CoSe<sub>4</sub>** were investigated by frequency- and temperature-dependent ac susceptibility measurements. With no static magnetic field applied, **CoS<sub>4</sub>** does not show temperature-dependent maxima in the out-of-phase magnetic susceptibility  $\chi''_M$  (Figure S6, SI), which are related to the relaxation time of the magnetization  $\tau$  through the relation  $\tau = (2\pi\nu)^{-1}$ . Upon application of a static magnetic field of 0.1 T, however, the spin dynamics are slowed down and the experimental detection of the relaxation times for different temperatures becomes possible (Figure S7, SI). The fitting of the  $\chi''_M(\nu)$  plots with the extended Debye model (see the Materials and Methods section) yields the temperature dependence of the relaxation times displayed in the left panel of Figure 4. A closely related behavior was found using static fields of 0.2 and 0.3 T (Figure S8, SI).

In order to check whether the observed dynamics have a single-molecular origin, as well as to address the role of intermolecular dipolar magnetic interactions in the zero field relaxation, a solid solution of **CoS<sub>4</sub>** in its diamagnetic Zn<sup>II</sup> analogue (**Co/ZnS<sub>4</sub>**) was prepared. X-ray powder diffraction analysis confirms the retention of the crystallographic space group and of the unit cell upon dilution (Figure S9, SI), and magnetometry indicates a 4 % molar ratio of the Co<sup>II</sup> species, close to the stoichiometry used in the synthesis. Unlike the case of **CoS<sub>4</sub>**, the ac susceptibility characterization of **Co/ZnS<sub>4</sub>** at zero static applied field reveals the presence of temperature-dependent maxima (Figures S10 and S11, SI, for 0 T and 0.1 T data, respectively). The corresponding relaxation times are reported in the left panel of Figure 4.

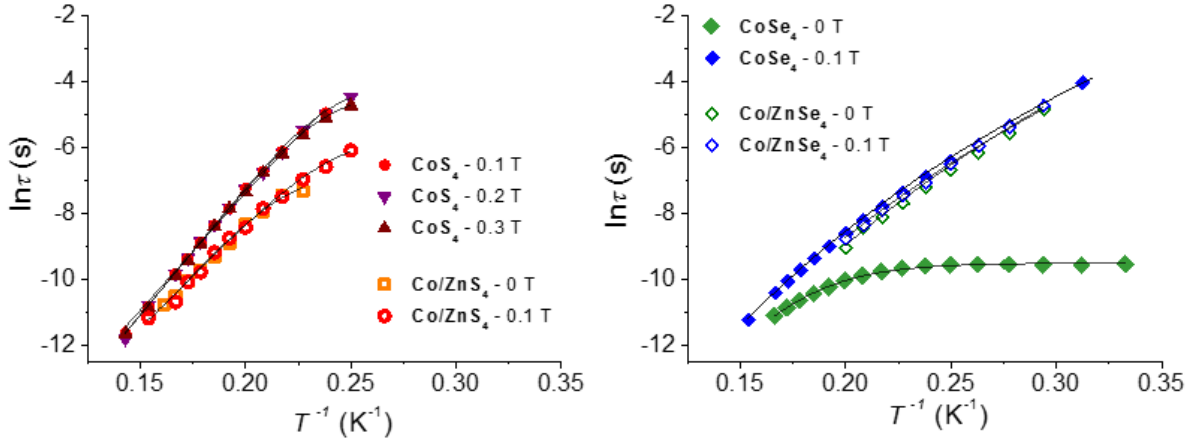


**Figure 4.** Arrhenius plot of the temperature dependence of the relaxation time of the magnetization for **CoS<sub>4</sub>**, **Co/ZnS<sub>4</sub>** (left), **CoSe<sub>4</sub>** and **Co/ZnSe<sub>4</sub>** (right), obtained from best fitting procedure of the isothermal  $\chi_M''(\nu)$ , as described in the Materials and Methods section. The lines represent the best-fits obtained as discussed in the text with parameters reported in Table 4.

The observed relaxation behavior indicates that intermolecular magnetic dipolar interactions provide an efficient relaxation pathway in the pure phase (undiluted sample) of **CoS<sub>4</sub>**. Suppressing these interactions upon dilution or application of a static magnetic field leads to the onset of an Arrhenius-like relaxation regime. The increase of the relaxation rate found for **Co/ZnS<sub>4</sub>** in a 0.1 T static field suggests the presence of a phonon-bottleneck effect.<sup>112</sup> Moreover, the deviation from linearity observed in the low temperature region for **CoS<sub>4</sub>** at applied fields of 0.1, 0.2 and 0.3 T, points out that a contribution from the phonon-mediated direct process cannot be completely ruled out, even if the overlapping of the curves indicates that this process is not the main one at this field region, since the corresponding rate should feature a  $B^4$  dependence.<sup>107</sup>

The temperature dependence of  $\tau$  was fitted by considering a multi-process model:

$$\tau_0^{-1}(T) = \tau_0^{-1} e^{\frac{-\Delta}{kT}} + CT^n + AT + QTM \quad (4)$$

In Equation (4,) several relaxation mechanisms are taken into account.<sup>107</sup> The first term describes an Orbach process, where the magnetization of the system decays through the thermally activated population of the  $|\pm 1/2\rangle$  Kramers doublet (in a classical picture, this term describe a phonon-induced overcome of the anisotropy barrier). In this case,  $\tau_0$  is a pre-exponential factor and  $\Delta$  is the height of the energy barrier. The second term relates to a Raman mechanism, where the  $|\pm 3/2\rangle$  states are coupled through a virtual one via a two-phonon process, and the third term relates to the direct coupling between the  $|\pm 3/2\rangle$  states. The last term stems from the quantum tunneling of the magnetization between the two sides of the magnetic anisotropy barrier, and has been used only for zero static field data. To reduce overparametrization, the data fitting procedure was addressed by including contributions of each process step by step, looking for the best fit obtained using the minimum number of processes. In particular, zero-field data were fitted constraining the direct term to zero, whereas for measurements in applied field, QTM was set to zero. For **CoS<sub>4</sub>**, the best fitting parameters are reported in Table 4. It is worth noting that the  $\Delta$  value is essentially in agreement with the expectations from static magnetic characterization (which provides an expected barrier of about 60 cm<sup>-1</sup>). The assumption that magnetic relaxation in this system actually occurs via the Orbach process, is reinforced by the impossibility of getting a reasonable fit by assuming the two-phonon process to be a Raman one.

Contrarily to **CoS<sub>4</sub>**, **CoSe<sub>4</sub>** turned out to be one of the very few examples of Co<sup>II</sup> complexes showing slow relaxation at zero field<sup>49,52,53,56,60,75</sup> (see Figure S12, SI). The relaxation times

obtained through the fitting of  $\chi_M''(\nu)$  are plotted in the right panel of Figure 4. In the higher range of investigated temperatures, **CoSe<sub>4</sub>** apparently follows an Arrhenius-like relaxation regime that gradually becomes temperature independent upon cooling. This behavior is in line with the dominance of QTM processes at the lowest temperatures. Application of a 0.1 T static magnetic field (Figure S13, SI), and dilution of **CoSe<sub>4</sub>** in its diamagnetic Zn<sup>II</sup> analogue (Figures S14-S16, SI), yield overlapping curves, which were tentatively fitted using Eq. (4) (best fit parameters reported in Table S2, SI). However, the best fit  $\Delta$  parameter (about 30 cm<sup>-1</sup>) is much lower than expected on the basis of static magnetic characterization (about 60 cm<sup>-1</sup>). This discrepancy cannot be traced back to QTM,<sup>78</sup> as often suggested in the literature, since Eq. (4) takes this process into account explicitly. This finding, combined with the non-strict linearity of the Arrhenius plot, suggests that the relaxation may actually occur via a combination of different processes. On the basis of the linearity of the log-log plot of  $1/\tau$  vs  $T$  (Figure S17, SI), and to keep the numbers of fitted parameters to a minimum, the observed temperature dependence of the relaxation rate (Figure 4, right) was thus fitted according to a Raman mechanism, including both a Raman and a QTM process (considered only for zero-field dynamics).<sup>113</sup> This provided a much better fit than the Orbach one, the corresponding parameters being reported in Table 4. A somehow large exponent ( $9 < n < 11$ ) is observed compared to that expected for a real Raman process, which should provide  $n = 9$ .<sup>107</sup> Such a difference can, however, be accounted for considering the Raman parameters as phenomenological, since they may well include the effects of otherwise discarded interactions, in particular, the hyperfine coupling to <sup>59</sup>Co ( $I = 7/2$ ) and residual dipolar intermolecular ones.<sup>72</sup>

**Table 4.** Magnetic relaxation parameters of the investigated systems, according to the different models described in the text.

	CoS4		Co/ZnS4			CoSe4		Co/ZnSe4		
<div><div></div><div><div><div></div><div></div></div></div></div>	Orbach mechanism					Raman mechanism				
	0.1 T	0.2 T	0.3 T	0 T	0.1 T	0 T	0.1 T	0 T	0.1 T	
	3.8(1) 10 <sup>-10</sup>	1.2(2) 10 <sup>-10</sup>	1.4(2) 10 <sup>-10</sup>	3(1) 10 <sup>-10</sup>	8(2) 10 <sup>-10</sup>	-	-	-	-	
	Δ (cm <sup>-1</sup> )	49(1)	54.2(9)	53.4(3)	47.6(2)	44(1)	-	-	-	-
	A (Hz K <sup>-1</sup> )	5(2)	15(3)	20(2)	-	63(5)	-	-	-	-
	C (Hz K <sup>-n</sup> )	-	-	-	-	-	2.9(7) 10 <sup>-3</sup>	4.4(2) 10 <sup>-4</sup>	1(1) 10 <sup>-4</sup>	5.3(8) 10 <sup>-4</sup>
	n	-	-	-	-	-	9.3(1)	10.11(3)	10.9(5)	10.13(9)
	QTM (kHz)	-	-	-	0.8(1)	-	13.7(2)	-	- <sup>a</sup>	-

<sup>a</sup>outside the experimentally accessible frequency range.

As a whole, the ac characterization clearly indicates that the behavior of undiluted **CoS<sub>4</sub>** and **CoSe<sub>4</sub>** is largely influenced by intermolecular dipolar magnetic coupling, which offers a powerful pathway for magnetic relaxation, as often reported in the literature of SIMs.<sup>53,114-116</sup> In the case of **CoS<sub>4</sub>**, such a relaxation pathway hinders the detection of slow relaxing magnetization, confirming that special care should be taken in analyzing potential SIMs in the undiluted phase. The larger contribution of QTM for **CoS<sub>4</sub>** than for **CoSe<sub>4</sub>**, both in pure and undiluted phase, is further in qualitative agreement with the observation of an EPR signal for the former and not for the latter.

## CONCLUSIONS

The analysis of static and dynamic magnetic properties of two Co<sup>II</sup>E<sub>4</sub>-containing, E = S, Se, complexes, combined with X-ray crystallography and EPR studies, unveiled the relevance of solid state effects in shaping the magnetic behavior of these systems. In particular, the crystal structure of **CoS<sub>4</sub>** and **CoSe<sub>4</sub>**, determined at low temperature, showed that, although the former complex has a more symmetrical first coordination sphere, it remarkably exhibits structural disorder in one of its peripheral 'Pr groups. Such disorder accounts for the presence of a signal in the HFEPR spectra of **CoS<sub>4</sub>**, which is attributed to the nominally forbidden  $\Delta M_S = \pm 3$  intra-doublet transition (i.e.  $D < 0$  for this system). The observation of this signal is compatible with a non-zero value of the rhombic parameter  $E$ , which would be unexpected in the absence of disorder, owing to the tetragonal space group of the **CoS<sub>4</sub>** crystals. On the other hand, **CoSe<sub>4</sub>** was found to be EPR silent, regardless of its less symmetrical first coordination sphere.

Contrarily to the tetrahedral Co<sup>II</sup> SIMs [Co(XPh)<sub>4</sub>]<sup>2-</sup> X = S, Se, dc magnetometry shows that the magnitude of  $D$  of **CoS<sub>4</sub>** and **CoSe<sub>4</sub>** is practically identical. Although this finding suggests that the corresponding ligand field strength does not affect the magnitude of  $D$ , we

cannot, at this stage, completely rule out a subtle balancing effect of the different ligand field strength and the slightly different structural features of the two complexes.

Analysis of the dynamics of the magnetization showed that **CoSe<sub>4</sub>** is one of the few examples of Co<sup>II</sup> complexes behaving as a SIM in the absence of a static magnetic field. Magnetic dilution of **CoS<sub>4</sub>** or **CoSe<sub>4</sub>** in the isostructural matrix of their Zn<sup>II</sup> analogues pinpoints the crucial role of intermolecular magnetic dipolar coupling in affecting this behavior. Finally, a comparative analysis of the static and dynamic magnetic characterization points out that, although the two complexes have a similar axial anisotropy, the corresponding spin dynamics apparently follow different mechanisms. The behavior of **CoS<sub>4</sub>** is best reproduced assuming an Orbach process over a thermal relaxation barrier, the magnitude of which is in good agreement with that estimated by magnetometry, whereas the behavior of **CoSe<sub>4</sub>** is best explained by assuming a dominant Raman contribution.

The present study is thus a *caveat* for the conventional design of SIMs, in which the geometry of the first coordination sphere and the nature of the donor atoms are often considered as lone actors in shaping the relaxation behavior of the systems. In addition, our findings highlight the necessity of multi-technique approaches for the complete characterization of molecular magnetic materials, including their structural characterization at temperatures comparable to those at which their magnetic properties are investigated.

Further development of this research activity should also encompass the synthesis and characterization of the as yet elusive [Co{<sup>i</sup>Pr<sub>2</sub>P(Te)NP(Te)<sup>i</sup>Pr<sub>2</sub>}<sub>2</sub>] complex, the feasibility of which is encouraged by previous studies of the corresponding Ni<sup>III17</sup> and Zn<sup>III18</sup> analogues. This

endeavor would also provide a testing experimental ground for the properties of  $[\text{Co}(\text{TePh})_4]^{2-}$ , which up to now have been investigated only *in silico*.<sup>80</sup>

## ACKNOWLEDGMENTS

This work was supported by the Special Account for Research Grants of the University of Athens (N.L., E.F., P.K.). The Fulbright Foundation in Greece and the National High Magnetic Field Laboratory via its Visiting Scientist Program supported an extended scientific visit of P.K. to the latter. HFEPR was performed at the NHMFL in Tallahassee, FL, USA, which is funded by NSF (Cooperative Agreement DMR 1157490), the State of Florida, and DOE. G.P., S.S. and L.S. gratefully acknowledge the financial contribution of the European Research Council through the Advanced Grant MolNanoMaS (267746) and of Italian MIUR through FIRB projects RBAP117RWN and RBFR10OAI0. G.P. and L.S. acknowledge fruitful discussions with Prof. R. Sessoli (University of Florence). Preliminary X-band EPR studies on **CoS<sub>4</sub>** and **CoSe<sub>4</sub>** had been carried out in the research group of Prof. E.J.J. Groenen (Leiden University), to whom we are grateful. Drs D. Maganas and A. Grigoropoulos are thanked by S.S., P.K. and P.K., respectively, for helpful discussions. We would like to thank all the Reviewers of the manuscript for their constructive comments.

## ASSOCIATED CONTENT

**Supporting Information.** HFEPR spectra of **CoS<sub>4</sub>** in the 56 – 406 GHz frequency range, HFEPR spectrum of a pellet of **CoS<sub>4</sub>**, UV-vis reflectance spectra of **CoS<sub>4</sub>** and **CoSe<sub>4</sub>**, field vs. frequency plot of HFEPR spectra of **CoS<sub>4</sub>** with simulations, isothermal magnetization curves of **CoS<sub>4</sub>** and **CoSe<sub>4</sub>** at low temperatures, powder X-ray diffraction data and complete ac set of data

for all the investigated samples, crystal data and crystallographic information files. This material is available free of charge via the Internet at <http://pubs.acs.org>.

## AUTHOR INFORMATION

### Corresponding Authors

giordano.poneti@gmail.com; kyritsis@chem.uoa.gr

## REFERENCES

1. Gatteschi, D.; Sessoli, R.; Villain, J. *Molecular Nanomagnets*; OUP Oxford, **2006**.
2. Sessoli, R.; Gatteschi, D.; Caneschi, A.; Novak, M. A. *Nature* **1993**, 365, 141.
3. Gatteschi, D.; Sessoli, R. *Angew. Chem., Int. Ed.* **2003**, 42, 268.
4. Wernsdorfer, W.; Sessoli, R. *Science* **1999**, 284, 133.
5. Gatteschi, D.; Cornia, A.; Mannini, M.; Sessoli, R. *Inorg. Chem.* **2009**, 48, 3408.
6. Bogani, L.; Wernsdorfer, W. *Nat. Mater.* **2008**, 7, 179.
7. Troiani, F.; Affronte, M. *Chem. Soc. Rev.* **2011**, 40, 3119.
8. Ishikawa, N.; Sugita, M.; Ishikawa, T.; Koshihara, S.; Kaizu, Y. *J. Am. Chem. Soc.* **2003**, 125, 8694.
9. Rinehart, J. D.; Long, J. R. *J. Am. Chem. Soc.* **2009**, 131, 12558.
10. Craig, G. A.; Murrie, M. *Chem. Soc. Rev.* **2015**, 44, 2135.
11. Frost, J.; Harriman, K. L. M.; Murugesu, M. *Chem. Science* **2016**, 7, 2470.
12. Bar, A. K.; Pichon, C.; Sutter, J. P. *Coord. Chem. Rev.* **2016**, 308, 346.
13. Ruiz, E.; Cirera, J.; Cano, J.; Alvarez, S.; Loose, C.; Kortus, J. *Chem. Commun.* **2008**, 52.

14. Neese, F.; Pantazis, D. A. *Faraday Discuss.* **2011**, *148*, 229.
15. Rinehart, J. D.; Long, J. R. *Chem. Science* **2011**, *2*, 2078.
16. Gomez-Coca, S.; Aravena, D.; Morales, R.; Ruiz, E. *Coord. Chem. Rev.* **2015**, *289*, 379.
17. Atanasov, M.; Aravena, D.; Suturina, E.; Bill, E.; Maganas, D.; Neese, F. *Coord. Chem. Rev.* **2015**, *289–290*, 177.
18. Accorsi, S.; Barra, A. L.; Caneschi, A.; Chastanet, G.; Cornia, A.; Fabretti, A. C.; Gatteschi, D.; Mortalo, C.; Olivieri, E.; Parenti, F.; Rosa, P.; Sessoli, R.; Sorace, L.; Wernsdorfer, W.; Zobbi, L. *J. Am. Chem. Soc.* **2006**, *128*, 4742.
19. Gregoli, L.; Danieli, C.; Barra, A.-L.; Neugebauer, P.; Pellegrino, G.; Poneti, G.; Sessoli, R.; Cornia, A. *Chem. Eur. J.* **2009**, *15*, 6456.
20. Totaro, P.; Westrup, K. C. M.; Boulon, M. E.; Nunes, G. G.; Back, D. F.; Barison, A.; Ciattini, S.; Mannini, M.; Sorace, L.; Soares, J. F.; Cornia, A.; Sessoli, R. *Dalton Trans.* **2013**, *42*, 4416.
21. Westrup, K. C. M.; Boulon, M. E.; Totaro, P.; Nunes, G. G.; Back, D. F.; Barison, A.; Jackson, M.; Paulsen, C.; Gatteschi, D.; Sorace, L.; Cornia, A.; Soares, J. F.; Sessoli, R. *Chem. Eur. J.* **2014**, *20*, 13681.
22. Freedman, D. E.; Harman, W. H.; Harris, T. D.; Long, G. J.; Chang, C. J.; Long, J. R. *J. Am. Chem. Soc.* **2010**, *132*, 1224.
23. Cornia, A.; Rigamonti, L.; Boccedi, S.; Clerac, R.; Rouzies, M.; Sorace, L. *Chem. Commun.* **2014**, *50*, 15191.
24. Deng, Y.-F.; Han, T.; Wang, Z.; Ouyang, Z.; Yin, B.; Zheng, Z.; Krzystek, J.; Zheng, Y.-Z. *Chem. Commun.* **2015**, *51*, 17688.

25. Ishikawa, R.; Miyamoto, R.; Nojiri, H.; Breedlove, B. K.; Yamashita, M. *Inorg. Chem.* **2013**, *52*, 8300.
26. Vallejo, J.; Pascual-Alvarez, A.; Cano, J.; Castro, I.; Julve, M.; Lloret, F.; Krzystek, J.; De Munno, G.; Armentano, D.; Wernsdorfer, W.; Ruiz-Garcia, R.; Pardo, E. *Angew. Chem., Int. Ed.* **2013**, *52*, 14075.
27. Grigoropoulos, A.; Pissas, M.; Papatolis, P.; Psycharis, V.; Kyritsis, P.; Sanakis, Y. *Inorg. Chem.* **2013**, *52*, 12869.
28. Craig, G. A.; Marbey, J. J.; Hill, S.; Roubeau, O.; Parsons, S.; Murrie, M. *Inorg. Chem.* **2015**, *54*, 13.
29. Sato, R.; Suzuki, K.; Minato, T.; Shinoe, M.; Yamaguchi, K.; Mizuno, N. *Chem. Commun.* **2015**, *51*, 4081.
30. Chen, L.; Wang, J.; Liu, Y.-Z.; Song, Y.; Chen, X.-T.; Zhang, Y.-Q.; Xue, Z.-L. *Eur. J. Inorg. Chem.* **2015**, 271.
31. Abhervé, A.; Palacios-Corella, M.; Clemente-Juan, J. M.; Marx, R.; Neugebauer, P.; van Slageren, J.; Clemente-Leon, M.; Coronado, E. *J. Mater. Chem. C* **2015**, *3*, 7936.
32. Pascual-Alvarez, A.; Vallejo, J.; Pardo, E.; Julve, M.; Lloret, F.; Krzystek, J.; Armentano, D.; Wernsdorfer, W.; Cano, J. *Chem. Eur. J.* **2015**, *21*, 17299.
33. Nemec, I.; Herchel, R.; Travnicek, Z.; Silha, T. *RSC Advances* **2016**, *6*, 3074.
34. Zadrozny, J. M.; Xiao, D. J.; Atanasov, M.; Long, G. J.; Grandjean, F.; Neese, F.; Long, J. R. *Nat. Chem.* **2013**, *5*, 577.
35. Dey, M.; Gogoi, N. *Angew. Chem., Int. Ed.* **2013**, *52*, 12780.

36. Samuel, P. P.; Mondal, K. C.; Amin Sk, N.; Roesky, H. W.; Carl, E.; Neufeld, R.; Stalke, D.; Demeshko, S.; Meyer, F.; Ungur, L.; Chibotaru, L. F.; Christian, J.; Ramachandran, V.; van Tol, J.; Dalal, N. S. *J. Am. Chem. Soc.* **2014**, *136*, 11964.
37. Harman, W. H.; Harris, T. D.; Freedman, D. E.; Fong, H.; Chang, A.; Rinehart, J. D.; Ozarowski, A.; Sougrati, M. T.; Grandjean, F.; Long, G. J.; Long, J. R.; Chang, C. J. *J. Am. Chem. Soc.* **2010**, *132*, 18115.
38. Atanasov, M.; Zadrozny, J. M.; Long, J. R.; Neese, F. *Chem. Science* **2013**, *4*, 139.
39. Eichhöfer, A.; Lan, Y.; Mereacre, V.; Bodenstein, T.; Weigend, F. *Inorg. Chem.* **2014**, *53*, 1962.
40. Mathoniere, C.; Lin, H.-J.; Siretanu, D.; Clerac, R.; Smith, J. M. *J. Am. Chem. Soc.* **2013**, *135*, 19083.
41. Bar, A. K.; Pichon, C.; Gogoi, N.; Duhayon, C.; Ramasesha, S.; Sutter, J.-P. *Chem. Commun.* **2015**, *51*, 3616.
42. Lin, P.-H.; Smythe, N. C.; Gorelsky, S. I.; Maguire, S.; Henson, N. J.; Korobkov, I.; Scott, B. L.; Gordon, J. C.; Baker, R. T.; Murugesu, M. *J. Am. Chem. Soc.* **2011**, *133*, 15806.
43. Mossin, S.; Tran, B. L.; Adhikari, D.; Pink, M.; Heinemann, F. W.; Sutter, J.; Szilagyi, R. K.; Meyer, K.; Mindiola, D. J. *J. Am. Chem. Soc.* **2012**, *134*, 13651.
44. Meng, Y.-S.; Mo, Z.; Wang, B.-W.; Zhang, Y.-Q.; Deng, L.; Gao, S. *Chem. Science* **2015**, *6*, 7156.
45. Miklovič, J.; Valigura, D.; Boča, R.; Titiš, J. *Dalton Trans.* **2015**, *44*, 12484.
46. Marriott, K. E. R.; Bhaskaran, L.; Wilson, C.; Medarde, M.; Ochsenbein, S. T.; Hill, S.; Murrie, M. *Chem. Science* **2015**, *6*, 6823.

47. Poulten, R. C.; Page, M. J.; Algarra, A. G.; Le Roy, J. J.; López, I.; Carter, E.; Llobet, A.; Macgregor, S. A.; Mahon, M. F.; Murphy, D. M.; Murugesu, M.; Whittlesey, M. K. *J. Am. Chem. Soc.* **2013**, *135*, 13640.
48. Lin, W.; Bodenstein, T.; Mereacre, V.; Fink, K.; Eichhöfer, A. *Inorg. Chem.* **2016**, *55*, 2091.
49. Zadrozny, J. M.; Long, J. R. *J. Am. Chem. Soc.* **2011**, *133*, 20732.
50. Vaidya, S.; Upadhyay, A.; Singh, S. K.; Gupta, T.; Tewary, S.; Langley, S. K.; Walsh, J. P. S.; Murray, K. S.; Rajaraman, G.; Shanmugam, M. *Chem. Commun.* **2015**, *51*, 3739.
51. Saber, M. R.; Dunbar, K. R. *Chem. Commun.* **2014**, *50*, 12266.
52. Fataftah, M. S.; Zadrozny, J. M.; Rogers, D. M.; Freedman, D. E. *Inorg. Chem.* **2014**, *53*, 10716.
53. Zadrozny, J. M.; Telser, J.; Long, J. R. *Polyhedron* **2013**, *64*, 209.
54. Yang, F.; Zhou, Q.; Zhang, Y.; Zeng, G.; Li, G.; Shi, Z.; Wang, B.; Feng, S. *Chem. Commun.* **2013**, *49*, 5289.
55. Cao, D.-K.; Feng, J.-Q.; Ren, M.; Gu, Y.-W.; Song, Y.; Ward, M. D. *Chem. Commun.* **2013**, *49*, 8863.
56. Ruamps, R.; Batchelor, L. J.; Guillot, R.; Zakhia, G.; Barra, A.-L.; Wernsdorfer, W.; Guihery, N.; Mallah, T. *Chem. Science* **2014**, *5*, 3418.
57. Rajnák, C.; Titiš, J.; Fuhr, O.; Ruben, M.; Boča, R. *Inorg. Chem.* **2014**, *53*, 8200.
58. Jurca, T.; Farghal, A.; Lin, P.-H.; Korobkov, I.; Murugesu, M.; Richeson, D. S. *J. Am. Chem. Soc.* **2011**, *133*, 15814.

59. Habib, F.; Luca, O. R.; Vieru, V.; Shiddiq, M.; Korobkov, I.; Gorelsky, S. I.; Takase, M. K.; Chibotaru, L. F.; Hill, S.; Crabtree, R. H.; Murugesu, M. *Angew. Chem., Int. Ed.* **2013**, *52*, 11290.
60. Zhu, Y.-Y.; Cui, C.; Zhang, Y.-Q.; Jia, J.-H.; Guo, X.; Gao, C.; Qian, K.; Jiang, S.-D.; Wang, B.-W.; Wang, Z.-M.; Gao, S. *Chem. Science* **2013**, *4*, 1802.
61. Colacio, E.; Ruiz, J.; Ruiz, E.; Cremades, E.; Krzystek, J.; Carretta, S.; Cano, J.; Guidi, T.; Wernsdorfer, W.; Brechin, E. K. *Angew. Chem., Int. Ed.* **2013**, *52*, 9130.
62. Vallejo, J.; Castro, I.; Ruiz-García, R.; Cano, J.; Julve, M.; Lloret, F.; De Munno, G.; Wernsdorfer, W.; Pardo, E. *J. Am. Chem. Soc.* **2012**, *134*, 15704.
63. Palion-Gazda, J.; Klemens, T.; Machura, B.; Vallejo, J.; Lloret, F.; Julve, M. *Dalton Trans.* **2015**, *44*, 2989.
64. Huang, X. C.; Zhou, C.; Shao, D.; Wang, X. Y. *Inorg. Chem.* **2014**, *53*, 12671.
65. Chen, L.; Wang, J.; Wei, J.-M.; Wernsdorfer, W.; Chen, X.-T.; Zhang, Y.-Q.; Song, Y.; Xue, Z.-L. *J. Am. Chem. Soc.* **2014**, *136*, 12213.
66. Diaz-Torres, R.; Menelaou, M.; Roubeau, O.; Sorrenti, A.; Brandariz-de Pedro, G.; Sanudo, E. C.; Teat, S.; Fraxedas, J.; Ruiz, E.; Aliaga, N. *Chem. Science* **2016**, *7*, 2793.
67. Rajnák, C.; Packová, A.; Titiš, J.; Miklovič, J.; Moncol, J.; Boča, R. *Polyhedron* **2016**, *110*, 85.
68. Zadrozny, J. M.; Liu, J.; Piro, N. A.; Chang, C. J.; Hill, S.; Long, J. R. *Chem. Commun.* **2012**, *48*, 3927.
69. Nedelko, N.; Kornowicz, A.; Justyniak, I.; Aleshkevych, P.; Prochowicz, D.; Krupiński, P.; Dorosh, O.; Ślawska-Waniewska, A.; Lewiński, J. *Inorg. Chem.* **2014**, *53*, 12870.
70. Herchel, R.; Váhovská, L.; Potočník, I.; Trávníček, Z. *Inorg. Chem.* **2014**, *53*, 5896.

71. Wu, D.; Zhang, X.; Huang, P.; Huang, W.; Ruan, M.; Ouyang, Z. W. *Inorg. Chem.* **2013**, *52*, 10976.
72. Gómez-Coca, S.; Urtizberea, A.; Cremades, E.; Alonso, P. J.; Camón, A.; Ruiz, E.; Luis, F. *Nat. Commun.* **2014**, *5*.
73. Boča, R.; Miklovič, J.; Titiš, J. *Inorg. Chem.* **2014**, *53*, 2367.
74. Shao, F.; Cahier, B.; Guihery, N.; Riviere, E.; Guillot, R.; Barra, A.-L.; Lan, Y.; Wernsdorfer, W.; Campbell, V. E.; Mallah, T. *Chem. Commun.* **2015**, *51*, 16475.
75. Carl, E.; Demeshko, S.; Meyer, F.; Stalke, D. *Chem. Eur. J.* **2015**, *21*, 1.
76. Smolko, L.; Černák, J.; Dušek, M.; Miklovič, J.; Titiš, J.; Boča, R. *Dalton Trans.* **2015**, *44*, 17565.
77. Chen, L.; Chen, S.-Y.; Sun, Y.-C.; Guo, Y.-M.; Yu, L.; Chen, X.-T.; Wang, Z.; Ouyang, Z. W.; Song, Y.; Xue, Z.-L. *Dalton Trans.* **2015**, *44*, 11482.
78. Rechkemmer, Y.; Breitgoff, F.D.; van der Meer, M.; Atanasov, M.; Hakl, M.; Orlita, M.; Neugebauer, P.; Neese, F.; Sarkar, B.; van Slageren, J. *Nat. Commun.* **2016**, *7*, 10467.
79. Ziegenbalg, S.; Hornig, D.; Görls, H.; Plass, W. *Inorg. Chem.*, **2016**, *55*, 4047.
80. Suturina, E. A.; Maganas, D.; Bill, E.; Atanasov, M.; Neese, F. *Inorg. Chem.* **2015**, *54*, 9948.
81. Silvestru, C.; Drake, J. E. *Coord. Chem. Rev.* **2001**, *223*, 117.
82. Ly, T. Q.; Woollins, J. D. *Coord. Chem. Rev.* **1998**, *176*, 451.
83. Haiduc, I. Dichalcogenoimidodiphosphinato Ligands in Comprehensive Coordination Chemistry II: From Biology to Nanotechnology, ed. J. A. McCleverty and T. J. Meyer, in Fundamentals, ed. A. B. P. Lever, 2004, Elsevier, Amsterdam, vol. 1, pp. 323–347.

84. Chivers, T.; Ritch, J. S.; Robertson, S. D.; Konu, J.; Tuononen, H. M. *Acc. Chem. Res.* **2010**, *43*, 1053.
85. Gilby, L. M.; Piggott, B. *Polyhedron* **1999**, *18*, 1077.
86. Maganas, D.; Staniland, S. S.; Grigoropoulos, A.; White, F.; Parsons, S.; Robertson, N.; Kyritsis, P.; Pneumatikakis, G. *Dalton Trans.* **2006**, 2301.
87. Maganas, D.; Milikisyants, S.; Rijnbeek, J. M. A.; Sottini, S.; Levesanos, N.; Kyritsis, P.; Groenen, E. J. J. *Inorg. Chem.* **2010**, *49*, 595.
88. Sottini, S.; Mathies, G.; Gast, P.; Maganas, D.; Kyritsis, P.; Groenen, E. J. J. *Phys. Chem. Chem. Phys.* **2009**, *11*, 6727.
89. Maganas, D.; Sottini, S.; Kyritsis, P.; Groenen, E. J. J.; Neese, F. *Inorg. Chem.* **2011**, *50*, 8741.
90. Cupertino, D.; Birdsall, D. J.; Slawin, A. M. Z.; Woollins, J. D. *Inorg. Chim. Acta* **1999**, *290*, 1.
91. Afzaal, M.; Crouch, D.; Malik, Mohammad A.; Motevalli, M.; O'Brien, P.; Park, J.-H.; Woollins, J. D. *Eur. J. Inorg. Chem.* **2004**, 171.
92. Cupertino, D.; Keyte, R.; Slawin, A. M. Z.; Williams, D. J.; Woollins, J. D. *Inorg. Chem.* **1996**, *35*, 2695.
93. Altomare, A.; Burla, M. C.; Camalli, M.; Cascarano, G. L.; Giacovazzo, C.; Guagliardi, A.; Moliterni, A. G. G.; Polidori, G.; Spagna, R. *J. Appl. Crystallogr.* **1999**, *32*, 115.
94. SHELXL-97, Programs for Crystal Structure Analysis, release 97–2, G. M. Sheldrick, University of Göttingen, Germany, **1998**.
95. Hassan, A. K.; Pardi, L. A.; Krzystek, J.; Sienkiewicz, A.; Goy, P.; Rohrer, M.; Brunel, L. C. *J. Magn. Reson.* **2000**, *142*, 300.

96. Cole, K. S.; Cole, R. H. *J. Chem. Phys.* **1941**, 9, 341.
97. Dekker, C.; Arts, A. F. M.; Dewijn, H. W.; Vanduyneveldt, A. J.; Mydosh, J. A. *Phys. Rev. B* **1989**, 40, 11243.
98. Gómez-Coca, S.; Cremades, E.; Aliaga-Alcalde, N.; Ruiz, E. *J. Am. Chem. Soc.* **2013**, 135, 7010-7018.
99. Cornia, A.; Sessoli, R.; Sorace, L.; Gatteschi, D.; Barra, A. L.; Daiguebonne, C. *Phys. Rev. Lett.* **2002**, 89, 257201.
100. Bouwen, A.; Caneschi, A.; Gatteschi, D.; Goovaerts, E.; Schoemaker, D.; Sorace, L.; Stefan, M. *J. Phys. Chem. B* **2001**, 105, 2658.
101. Zhu, Y.-Y.; Yin, T.-T.; Jiang, S.-D.; Barra, A.-L.; Wernsdorfer, W.; Neugebauer, P.; Marx, R.; Dörfel, M.; Wang, B.-W.; Wu, Z.-Q.; van Slageren, J.; Gao, S. *Chem. Commun.*, **2014**, 50, 15090.
102. Barra, A.-L.; Caneschi, A.; Gatteschi, D.; Sessoli, R.; *J. Am. Chem. Soc.* **1995**, 117, 8855.
103. Goldberg, D.P.; Telser, J.; Krzystek, J.; Montalban, A.G.; Brunel, L. C.; Barrett, A.G.M.; Hoffman, B.M. *J. Am. Chem. Soc.* **1997**, 119, 8722.
104. Aubin, S.M.J.; Sun, Z.; Pardi, L.; Krzystek, J.; Folting, K.; Brunel, L.-C.; Rheingold, A.L.; Christou, G.; Hendrickson, D.N. *Inorg. Chem.* **1999**, 38, 5329.
105. Westrup, K.C.M.; Boulon, M.-E.; Totaro, T.; Nunes, G.G.; Back, D.F.; Barison, A.; Jackson, M.; Paulsen, C.; Gatteschi, D.; Sorace, L.; Cornia, A.; Soares, J.F.; Sessoli, R. *Chem. Eur. J.* **2014**, 20, 13681.
106. Pilbrow, J. R. *J. Magn. Reson.* **1978**, 31, 479.
107. Carlin, R. L. *Magnetochemistry*; Springer-Verlag, **1986**.

108. Chilton, N. F.; Anderson, R. P.; Turner, L. D.; Soncini, A.; Murray, K. S. *J. Comput. Chem.* **2013**, *34*, 1164.
109. Boča, R. *Coord. Chem. Rev.* **2004**, *248*, 757.
110. Davison, A.; Switkes, E.S. *Inorg. Chem.* **1971**, *10*, 837.
111. Fukui, K.; Kojima, N.; Ohyanishiguchi, H.; Hirota, N. *Inorg. Chem.* **1992**, *31*, 1338.
112. Schenker, R.; Leuenberger, M. N.; Chaboussant, G.; Loss, D.; Güdel, H. U. *Phys. Rev. B* **2005**, *72*, 184403
113. Tesi, L.; Lucaccini, E.; Cimatti, I.; Perfetti, M.; Mannini, M.; Atzori, M.; Morra, E.; Chiesa, M.; Caneschi, A.; Sorace, L.; Sessoli, R. *Chem. Sci.* **2016**, *7*, 2074.
114. Meihaus, K. R.; Rinehart, J. D.; Long, J. R. *Inorg. Chem.* **2011**, *50*, 8484.
115. Huang, W.; Liu, T.; Wu, D.; Cheng, J.; Ouyang, Z.W.; Duan, C. *Dalton Trans.* **2013**, *42*, 15326.
116. Habib, F.; Korobkov, I.; Murugesu., M. *Dalton Trans.* **2015**, *44*, 6368.
117. Levesanos, N.; Robertson, S.D.; Maganas, D.; Raptopoulou, C.P.; Terzis, A.; Kyritsis, P.; Chivers, T. *Inorg. Chem.* **2008**, *47*, 2949.
118. Chivers, T.; Eisler, D.J.; Ritch J.S. *Dalton Trans.* **2005**, 2675.